Amyloid-related Imaging Abnormalities in Alzheimer Disease Treated with Anti–Amyloid-β Therapy

Amit Agarwal, MD • Vivek Gupta, MD • Pavan Brahmbhatt, MD • Amit Desai, MD • Prasanna Vibhute, MD
Nelly Joseph-Mathurin, PhD • Girish Bathla, MD

Author affiliations, funding, and conflicts of interest are listed at the end of this article.
See the invited commentary by Yu in this issue.

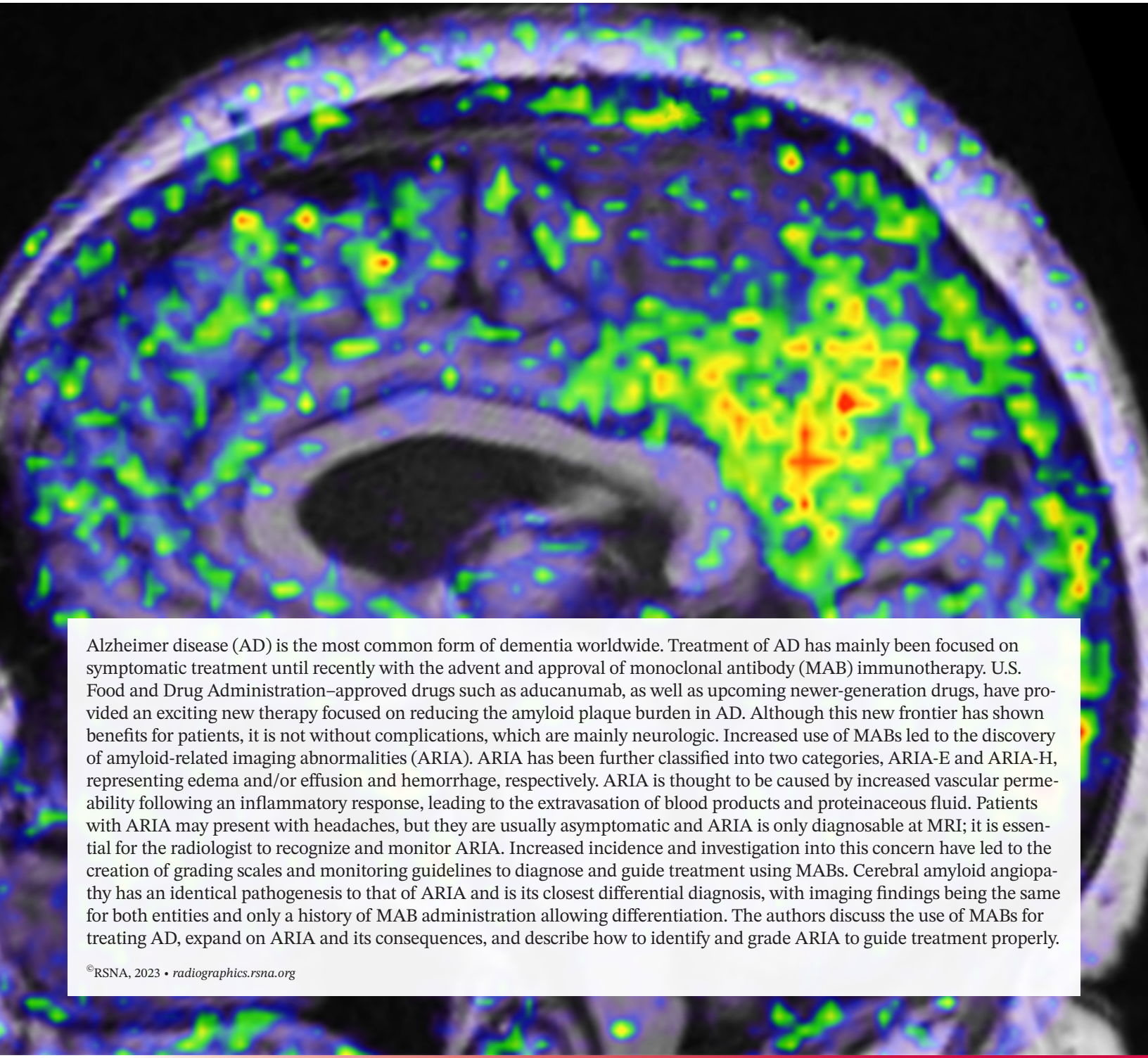

Alzheimer disease (AD) is the most common form of dementia worldwide. Treatment of AD has mainly been focused on symptomatic treatment until recently with the advent and approval of monoclonal antibody (MAB) immunotherapy. U.S. Food and Drug Administration–approved drugs such as aducanumab, as well as upcoming newer-generation drugs, have provided an exciting new therapy focused on reducing the amyloid plaque burden in AD. Although this new frontier has shown benefits for patients, it is not without complications, which are mainly neurologic. Increased use of MABs led to the discovery of amyloid-related imaging abnormalities (ARIA). ARIA has been further classified into two categories, ARIA-E and ARIA-H, representing edema and/or effusion and hemorrhage, respectively. ARIA is thought to be caused by increased vascular permeability following an inflammatory response, leading to the extravasation of blood products and proteinaceous fluid. Patients with ARIA may present with headaches, but they are usually asymptomatic and ARIA is only diagnosable at MRI; it is essential for the radiologist to recognize and monitor ARIA. Increased incidence and investigation into this concern have led to the creation of grading scales and monitoring guidelines to diagnose and guide treatment using MABs. Cerebral amyloid angiopathy has an identical pathogenesis to that of ARIA and is its closest differential diagnosis, with imaging findings being the same for both entities and only a history of MAB administration allowing differentiation. The authors discuss the use of MABs for treating AD, expand on ARIA and its consequences, and describe how to identify and grade ARIA to guide treatment properly.

Invited Commentary

RadioGraphics 2023; 43(9):e230009
https://doi.org/10.1148/rg.230009

Content Codes: MR, NM, NR

Quiz questions for this article are available through the Online Learning Center

Abbreviations: AD = Alzheimer disease, Aβ = amyloid β, ARIA = amyloid-related imaging abnormalities, ARIA-E = ARIA edema and/or effusion, ARIA-H = ARIA hemorrhage, CAA = cerebral amyloid angiopathy, CAA-RI = CAA-related inflammation, CSF = cerebrospinal fluid, FDA = U.S. Food and Drug Administration, FLAIR = fluid-attenuated inversion-recovery, GRE = gradient-recalled echo, MAB = monoclonal antibody, PRES = posterior reversible encephalopathy syndrome

TEACHING POINTS

- Accumulation of Aβ in the brain is the primary underlying process driving AD pathogenesis with the rest of the disease process, like neurofibrillary τ tangles resulting from an imbalance between Aβ production and clearance.
- While FDG PET is a vital tool in imaging for AD, newer amyloid-specific tracers and τ-specific tracers have both increased specificity and sensitivity when compared with those of FDG. These tracers allow earlier identification of plaque buildup even before patients become symptomatic and potentially allow earlier intervention.
- Dosage and *APOE-e4* carrier status are the most important risk factors for developing ARIA, and even with dose titration, ARIA usually occurs early. The presence of *APOE-e4* leads to increased plaque deposition and a significantly higher incidence of ARIA.
- ARIA-E should be the number one diagnostic consideration when parenchymal edema and/or sulcal FLAIR hyperintensity is seen in patients recently exposed to an amyloid-modifying MAB and in whom no evidence of any other inciting cause or underlying lesion can be found.
- Continuation of therapy in patients with ARIA relies heavily on the radiologist properly grading and monitoring the imaging findings. In many cases, therapy may continue in asymptomatic patients. ARIA-E is more transient, and therapy may continue or be temporarily stopped; stoppage of therapy in patients with ARIA-H depends on the severity and whether it is stabilized.

Introduction

Alzheimer disease (AD) is a progressive irreversible brain disorder that slowly degrades memory and cognitive function and is the most common form of dementia worldwide (1). While earlier treatment methods focused on symptomatic control, recent approvals of monoclonal antibodies (MABs), a set of disease-modifying drugs, have provided a way to target the pathogenesis itself (1,4). The main pathologic feature of AD is an aggregation of toxic amyloid B (Aβ). Disease-modifying drugs work by clearing toxic Aβ protein from the brain (1,2). In June 2021, the U.S. Food and Drug Administration (FDA) gave accelerated approval for aducanumab (Aduhelm; Biogen) as a treatment of AD, marking a paradigm shift in the treatment approach. This is the first treatment directed at the underlying pathophysiologic process with a reduction in Aβ. The FDA has determined that there is substantial evidence that aducanumab reduces Aβ plaques in the brain and that the reduction in these plaques is likely to result in benefits to patients (3,4).

Recently, a phase III trial of a newer MAB, lecenemab, displayed a reduction in cognitive decline, further strengthening the support for MABs (5,6). Major safety concerns from this category of medications were neurologic and classified as amyloid-related imaging abnormalities (ARIA). ARIA can be further divided into two broad categories: hemorrhage (ARIA-H) and edema and/or effusion (ARIA-E). Lacenemab showed an incidence of around 21% for these complications (3–5,7–9). As MRI is the only modality that can be used to diagnose these side effects, the International Collaboration for Real-World Evidence in Alzheimer's Disease (ICARE-AD) established guidelines for baseline imaging and serial monitoring (10). As MABs become more widespread, close collaboration between neurologists and radiologists is needed before and during therapy to plan for image monitoring as per guidelines. For radiologists, knowledge about the imaging findings of ARIA and the imaging protocol is essential, as the volume of treatment-monitoring MRI examinations is expected to grow exponentially over the next decade.

Neuropathology of AD

The two primary lesions associated with AD are senile plaques and neurofibrillary tangles (Fig 1). Senile plaques are extracellular nonvascular aggregates of Aβ, more specifically Aβ-40 and Aβ-42. Senile plaques are derived from the abnormal processing of amyloid precursor protein by the β- and γ-secretases, resulting in an imbalance in the production and clearance pathways (1,11–14). Aβ monomers are cleared through enzymatic breakdown and perivascular drainage but may aggregate into larger protein complexes like oligomers, protofibrils, and mature fibrils. Eventually, these complexes deposit in the brain as amyloid plaques (11,12,14). The Aβ-40 prototype tends to deposit in the vessel wall and forms the pathologic basis of cerebral amyloid angiopathy (CAA), whereas the Aβ-42 deposits in the brain parenchyma as the primary AD plaques. Neurofibrillary tangles are the second hallmark of AD, characterized by intraneuronal protein inclusions resulting from misfolded and abnormally phosphorylated τ protein aggregation. Neurofibrillary tangles are most commonly seen in the entorhinal cortex and hippocampal system and have the lowest concentration in the sensorimotor regions (1,11,13).

In 2018, the National Institute on Aging and Alzheimer's Association (NIA-AA) research framework moved to an objective biologic definition of AD where the underlying pathologic processes could be documented during postmortem examination or by in vivo biomarkers (15). Autopsy remains the standard for diagnosis, and the NIA-AA uses the ABC scoring system for AD neuropathologic changes. This is based on a composite of the Thal stage of amyloid deposition (A), the Braak stage of neurofibrillary tangles (B), and the Consortium to Establish a Registry for AD (CERAD) neuritic plaque score (C) (Fig 2A). The "cascade hypothesis" postulates that the accumulation of Aβ in the brain is the primary underlying process driving AD and sets the stage for further aggregation (16). It is now believed that amyloid plaque deposition is the critical initial step in AD pathophysiology (17). Moreover, diffuse plaques and benign plaques occur much earlier than do neuritic plaques, thus supporting the idea of therapeutic intervention in the early stage of the disease with a focus on decreased production or increased clearance of Aβ (Fig 2B–2D) (1,11,15). Accumulation of Aβ in the brain is the primary underlying process driving AD pathogenesis with the rest of the disease process, like neurofibrillary tangles resulting from an imbalance between Aβ production and clearance.

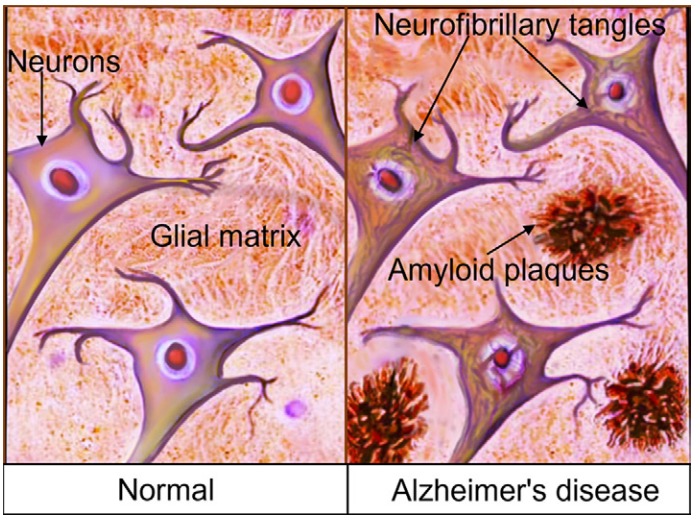

Figure 1. Primary pathophysiology of AD. The two primary lesions associated with AD are extracellular nonvascular aggregates of Aβ (senile plaques) and intraneuronal protein inclusions secondary to aggregation of misfolded and abnormally phosphorylated protein τ (neurofibrillary tangles).

Updates in Imaging AD

In 2018, with the creation of the AD research framework, numerous imaging and cerebrospinal fluid (CSF) biomarkers have been recognized (15). The revised definition scheme is based on three groups of biomarkers instead of the two groups used in the earlier 2011 recommendation: amyloid and τ (A and T, respectively). The new criteria labeled as AT(N) are based on aggregates of Aβ, τ (neurofibrillary tangles), and neurodegeneration or neuronal injury (N). CSF Aβ-42, or Aβ-42/Aβ-40 ratio, and amyloid PET are markers for A. CSF phosphorylated τ and τ PET are markers for T; anatomic MRI, fluorine 18 (^{18}F) fluorodeoxyglucose (FDG) PET, and CSF total τ serve as markers for N (15). Each category is therefore defined by an imaging and CSF biomarker. The term *Alzheimer disease* can be used only if biomarker evidence of both Aβ and pathologic τ is present, independent of clinical symptoms.

PET is increasingly recognized as a vital tool for earlier diagnosis of neurodegenerative conditions, most commonly by using ^{18}F-FDG. FDG estimation of brain glucose metabolism is nonspecific, and an emerging class of radiotracers targeting AD-specific proteins, including Aβ and τ, are offering more specific information than conventional structural (MRI) and nuclear (FDG PET) imaging (18–20). With the advent of PET/MRI, a single examination can provide information about two of the three defined A/T/N categories. Amyloid CT/MRI-PET is widely used for AD with multiple FDA-approved tracers, including carbon 11 (^{11}C)–labeled Pittsburgh compound-B, carbon 18 (^{18}C)–labeled florbetapir, and ^{18}C-labeled flutemetamol. The sensitivity of amyloid PET for AD detection has been reported to be 60%–100%, with most studies reporting sensitivities greater than 90% (Fig 3A, 3B) (19,21,22). Although a large and wide variety of τ PET ligands exist, ^{18}F-flortaucipir is the only one that is FDA approved, with limited availability at a few major medical centers (18,19). τ PET also has shown a strong ability to discriminate AD from other neurodegenerative disorders, with sensitivity and specificity around 90% and 95%, respectively (23). Second-generation τ tracers like RO948 will likely provide even higher levels of specificity once they are FDA approved, although more studies are needed (22,24).

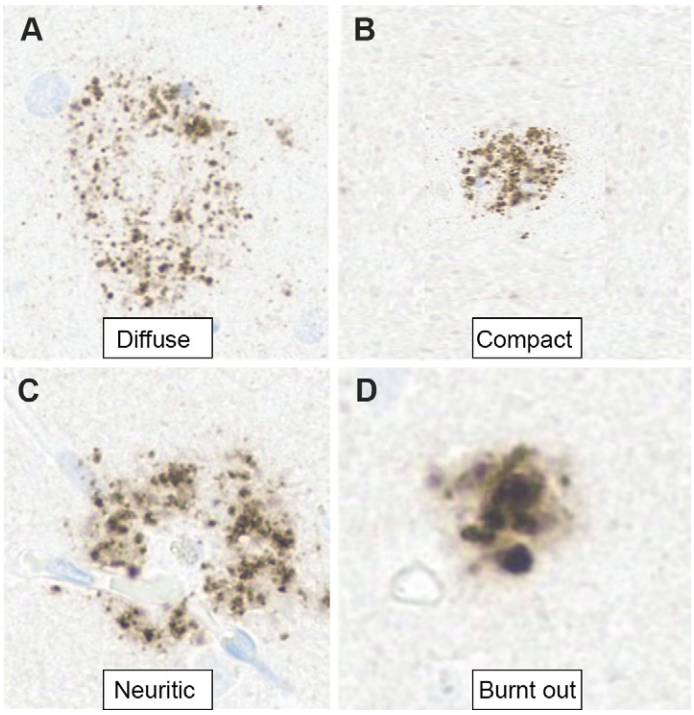

Figure 2. Photomicrographs show the evolution of Aβ plaques in AD. **(A)** Diffuse plaques are usually nonneuritic and not associated with glial responses or synaptic loss. **(B, C)** Compact (dense) plaques **(B)** activate the microglial cells with associated synaptic loss, eventually surrounded by dystrophic neurites known as neuritic plaques **(C)**. **(D)** "Burnt-out" plaques are end-stage plaques that do not show any accompanying dystrophic neurites. Brain accumulation of even diffuse Aβ, however, initiates the AD process (cascade hypothesis), thus supporting the idea of a therapeutic intervention in the early stage of the disease. (Aβ immunohistochemistry stain; 10 μm.)

While FDG PET is a vital tool in imaging for AD, newer amyloid-specific tracers and τ-specific tracers have both increased specificity and sensitivity when compared with those of FDG. These tracers allow earlier identification of plaque buildup even before patients become symptomatic and potentially allow earlier intervention.

Emerging Therapies for AD: What Is on the Horizon?

Most of the currently approved treatments for AD aim to improve cognitive symptoms without altering the underlying course of the disease, best exhibited by cholinesterase inhibitors like donepezil. Donepezil exerts its effect by increasing levels of available acetylcholine to compensate for the loss of functioning cholinergic brain cells (2). The cascade hypothesis implies that amyloid plaque deposition is the main pathogenesis, setting the stage for other secondary events (16). Therefore, most recent trials have focused on stopping amyloid plaque formation and facilitating its removal. This led to the discovery of MABs as disease-modifying agents (2,3,5,6). For a long time, it was assumed that aggregated Aβ in the extracellular space was responsible for the cytotoxic effects on neurons. However, there is increasing evidence that prefibrillar soluble forms of Aβ are also pathogenic and can cause neuronal injury (Fig 4A) (2,11,12). The Aβ-42 form has a higher tendency to oligomerize

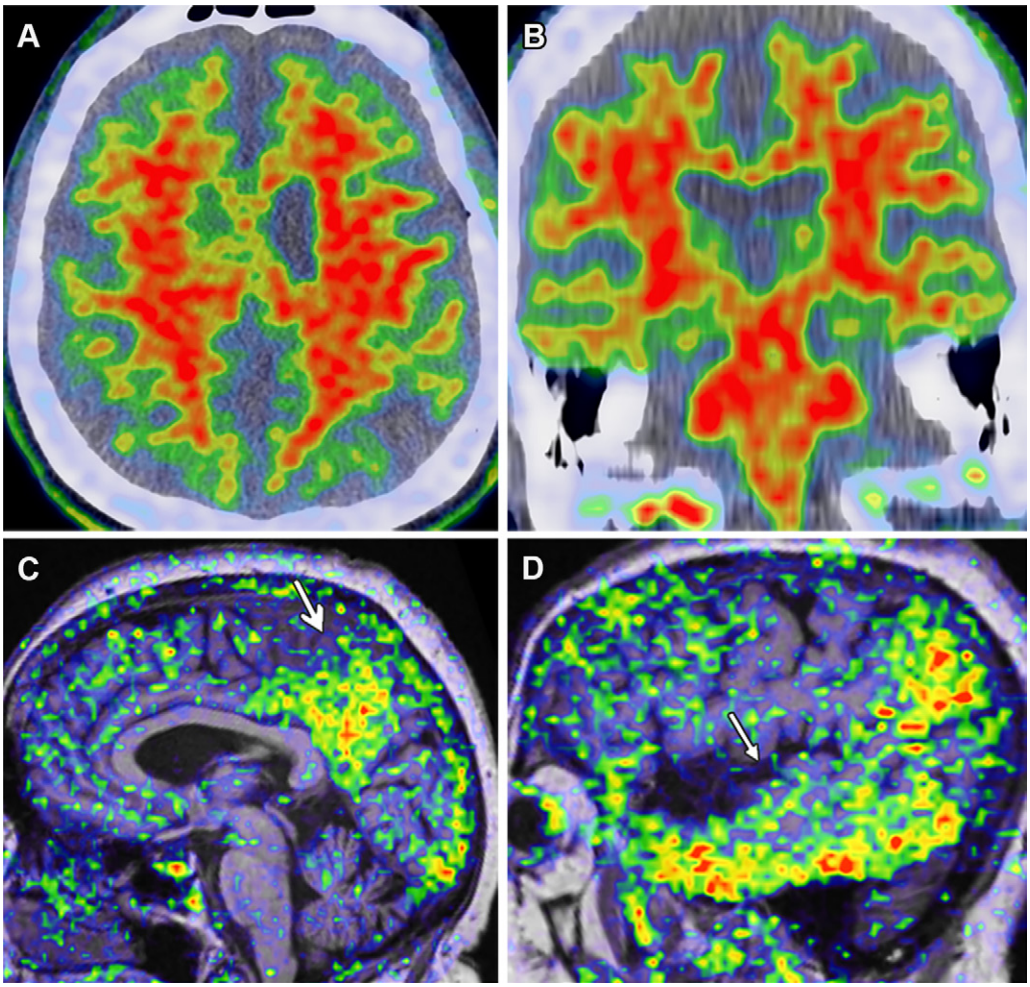

Figure 3. Amyloid and τ PET imaging in AD in a 72-year-old man with AD dementia. **(A, B)** Axial **(A)** and coronal **(B)** PET/CT amyloid images (tracer: florbetapir) show extensive diffuse uptake in the bilateral frontoparietal and temporal lobes. **(C, D)** Midsagittal **(C)** and lateral sagittal **(D)** MRI/PET τ images (tracer: AV-1451) show moderate uptake (arrow) in the temporoparietal lobe including the precuneus and posterior cingulate, representing τ deposits. Although overlap between the τ and amyloid tracers is present, abundant uptake is seen in the lateral temporal lobes with the τ ligand but not with the amyloid ligand.

and form amyloid fibrils than the more abundant Aβ-40 peptide (2,11,12). Passive immunization with MABs facilitates Aβ clearance by unbundling the amyloid bundles and through microglia or complement activation (Fig 4B) (8,25).

In June 2021, after almost 2 decades, the FDA approved a new AD medication, aducanumab, an antiamyloid MAB. Aducanumab is the first and only MAB directed against Aβ to be approved by the FDA for treating AD (3). Subsequently, trials for many other MABs (donanemab, gantenerumab) are near completion and should be available for clinical use soon. Lacenemab recently completed the phase III trial with positive results and has now been FDA approved (6). Aducanumab has only been approved for patients with mild cognitive impairment and mild dementia, with its role in severe and advanced AD still being studied.

ARIA: Definition and Mechanism

The Alzheimer's Association Research Roundtable convened a working group in 2010 to provide information and recommendations regarding the imaging abnormalities encountered in the antiamyloid trials. The working group included academic and industry representatives and was tasked with providing expert advice regarding FDA concerns related to imaging abnormalities associated with MABs. This working group termed these abnormalities *amyloid-related imaging abnormalities*, with ARIA-E for edema and/or effusion and ARIA-H for hemorrhage (microhemorrhages and superficial siderosis) (9).

AD is characterized by increased parenchymal Aβ accumulation and reduced perivascular clearance, resulting in increased Aβ in the vessel wall and disrupted smooth muscle cells (8,26). As AD progresses, cerebral vessels accumulate significant amyloid, disrupting vascular integrity and impairing perivascular Aβ clearance pathways (1,11,12). After anti-Aβ therapy initiation, vessels with preexisting amyloid vascular pathologic conditions become more susceptible to vascular extravasation events, resulting in ARIA-E (leakage products of proteinaceous fluid) and ARIA-H (blood products leaking through damaged vessel walls) (9,27). The degree of increased vascular permeability depends on the severity of preexisting amyloid angiopathy, the efficiency of amyloid clearance, and the local inflammatory response (Fig 5) (9,25,27).

The role of Aβ deposition in both CAA and AD is an excellent example of cross talk between neurodegenerative and cerebrovascular diseases with a common underlying mechanism. ARIA seen in trials of anti-Aβ immunotherapy are yet another example of an intersection between CAA and AD, representing an overload of perivascular clearance pathways and the effects of removing Aβ from CAA-positive vessels (7,8,25,28). Although Aβ is the main component of neuritic

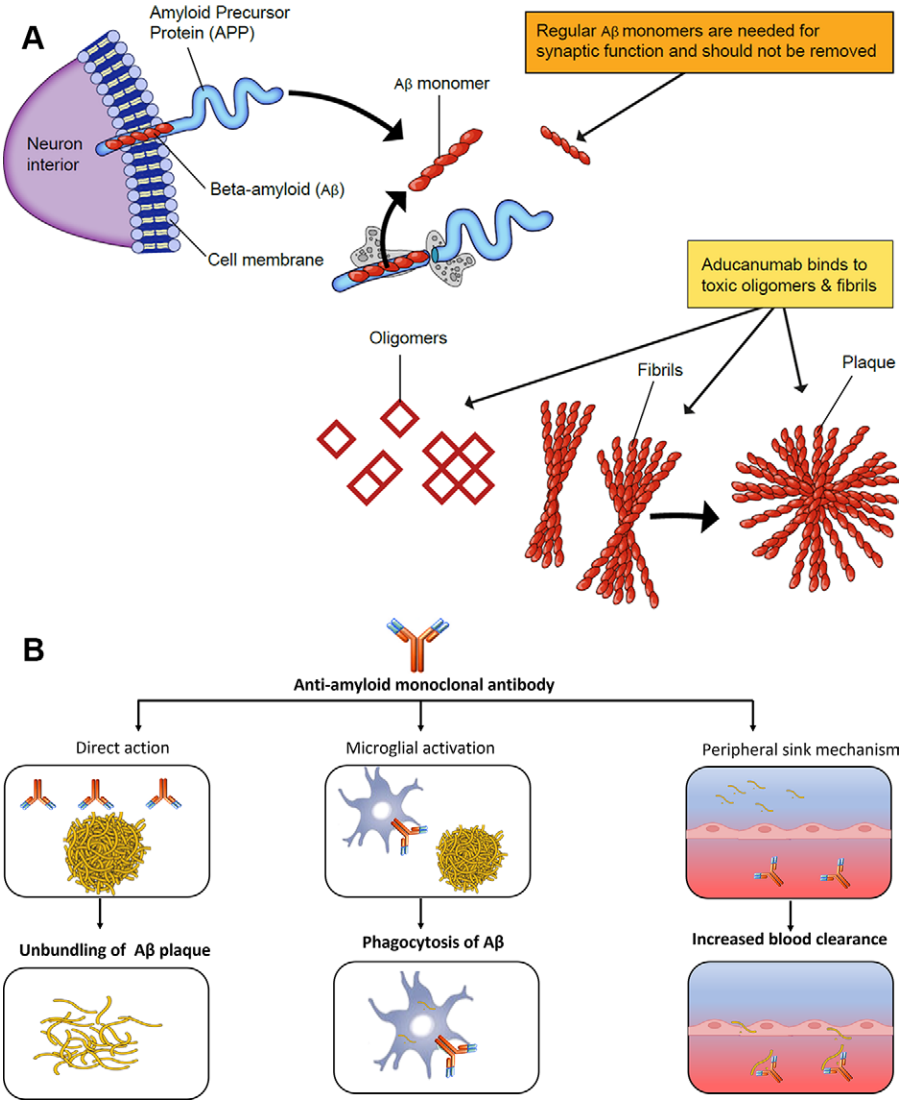

Figure 4. Mechanism of action of aducanumab (antiamyloid MAB). Aβ monomers are needed for regular synaptic functions. However, the oligomers and fibrils set off a cascade chain reaction resulting in neuronal loss and are the primary targets of aducanumab **(A)**. This includes direct action on the amyloid plaque with unbundling, activation of microglial-induced phagocytosis, and increased blood clearance **(B)**.

plaques and CAA, the length of Aβ peptide deposits is different, with Aβ-42 mainly deposited in neuritic plaques and the shorter Aβ-40 being the predominant form deposited in vessel walls (11,28). The relationship is more complex as the ARIA inflammatory response decreases over treatment, unlike the independent progression of CAA.

The clinical presentations of ARIA and CAA are different. Although there are currently minimal data regarding the clinical course associated with ARIA, patients with CAA-related inflammation (CAA-RI) are commonly symptomatic and present with cognitive decline, seizures, and headaches. In contrast, most patients with ARIA are asymptomatic and identified at monitoring MRI examinations (28–30).

Risk Factors, Dose Titration, and Timeline

Apart from the drug dosage, apolipoprotein E *(APOE-e4)* allele carriership and the presence of pretreatment hemorrhage (microhemorrhage and siderosis) are the most critical risk factors for ARIA (4,9,31–33). A strong correlation was found between drug dosage and the presence of ARIA, and most cases of ARIA developed during dose titration or after achieving the target dose. It is standard practice to start at a low dose of 1 mg/kg for the first two infusions, moving to 3 mg/kg for the third and fourth infusions, 6 mg/kg for the fifth and sixth infusions, and finally to the optimum target dosage of 10 mg/kg from beyond the seventh infusion (4). Titration is usually done over a period of 20–24 weeks. The target 10 mg/kg dose is administered as an intravenous infusion over approximately 1 hour every 4 weeks. Despite dose titration, most cases of ARIA are seen within the first eight doses during the transient phase of presumed loss of vessel wall integrity (4,32,33).

APOE-e4 allele carriership is the second most potent risk factor for developing ARIA. One of the most extensive phase III studies evaluating aducanumab (EMERGE and ENGAGE) showed an increased risk of ARIA-E with *APOE-e4* allele carriership and pretreatment hemorrhage, with no increase in risk for ARIA-H (4). Other studies contradict this finding and have shown an increased risk for both ARIA-E and ARIA-H with these risk factors (34,35). *APOE-e4* is a significant genetic risk factor for AD and CAA, contributing to Aβ deposition and clearance, τ phosphorylation, and associated neuroinflammation. Given the high risk, some studies have proposed *APOE-e4* genetic testing before MAB therapy and a higher frequency of monitoring image examinations.

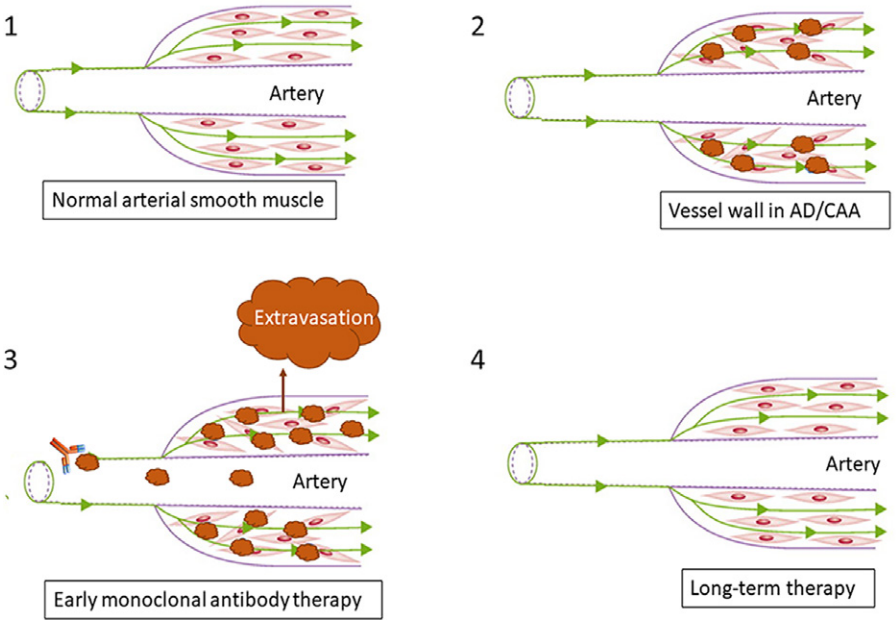

Figure 5. Pathophysiology of ARIA. Increased parenchymal Aβ accumulation with reduced perivascular clearance along with Aβ deposition within the vessel wall is seen in AD and CAA, resulting in disruption of arterial smooth muscle *(1, 2)*. After anti-Aβ therapy initiation, vessels with preexisting amyloid vascular pathologic conditions become more susceptible to vascular extravasation events, resulting in ARIA-E (leakage of proteinaceous fluid) and ARIA-H (leakage of blood products) *(3)*. Long-term therapy results in clearance of vessel wall amyloid buildup with reorganization of arterial smooth muscle *(4)*.

Most studies have shown a significantly higher incidence of ARIA-E, ranging around 30%–35% in the early part of treatment compared with approximately 15%–20% for ARIA-H (4,5,32,35). Although most cases (roughly 74%) are asymptomatic and discovered at MRI, headache is the most common clinical symptom with ARIA, with other less common manifestations being encephalopathy and falls (4,9,31). The working group supports the recommendation that the cutoff value of four microhemorrhages is used for exclusion in trials of amyloid-modifying therapies for AD. This may change with time as more information is available (9).

Dosage and *APOE-e4* carrier status are the most important risk factors for developing ARIA, and even with dose titration, ARIA usually occurs early. The presence of *APOE-e4* leads to increased plaque deposition and a significantly higher incidence of ARIA.

MRI Acquisition Protocol

ICARE-AD is a prospective, single-arm, multicenter, real-world observational study to evaluate the safety and efficacy of aducanumab across more than 200 centers in the United States. ICARE-AD has proposed an MRI protocol that includes details on the pulse sequences and the timeline to maintain consistency for detecting ARIA. The summary of the protocol (Fig 6) includes a baseline (pretreatment) imaging examination, a posttreatment imaging examination before the seventh and 12th infusions, and imaging every 6–12 months after that for up to 5 years. The mandatory sequences outlined in Table 1 include three-dimensional (3D) T2-weighted fluid-attenuated inversion-recovery (FLAIR), T2*-weighted gradient-recalled echo (GRE), and diffusion-weighted imaging. The FLAIR sequence forms the mainstay for diagnosing ARIA-E, and GRE sequences are used to monitor hemorrhagic contents. A section thickness of 5 mm or less is recommended for all sequence types (9,10). Sensitivity to detect microhemorrhage and siderosis increases with MRI scanner strength, longer echo times, and lower readout bandwidth.

Apart from the standardization of protocol, another essential factor is the standardization of magnet strength. While high-field-strength MRI scanners are likely to have greater sensitivity, the use of 1.5-T scanners is endorsed as a minimum standard, recognizing that the availability of higher-field scanners is limited to specific centers. If a center has easy availability to high-field scanners (3-T or 7-T magnets), it is imperative to maintain consistency, not only with the field strength but also with the vendor type. This requires close collaboration with the clinical team (neurologists), schedulers, and neuroradiologists. Every center should identify a few trained neuroradiologists to lead this effort with close communication, as even one wrong imaging examination can derail the entire monitoring process. Although ARIA can occur anytime, clinical suspicion for ARIA should be highest early in treatment (4,8,9,34,35).

Routine surveillance MRI should be supplemented with ad hoc MRI in patients with new-onset symptoms potentially associated with ARIA. This careful monitoring can help detect ARIA early. Patient counseling (preferably by the clinical team and/or neurologist) regarding ARIA is recommended to avoid unnecessary alarm related to imaging results. This can be described to patients as "temporary swelling" in the brain and as "spots of bleeding" in or on the surface of the brain. Patients should also be counseled at the same time that most of these imaging manifestations are clinically silent, and it is expected for the patient to be asymptomatic despite having positive MRI findings.

ARIA Edema and/or Effusion

ARIA-E is characterized by parenchymal edema and/or sulcal effusion and remains the most common side effect of MABs (4,31,36). In the two phase III trials (EMERGE and ENGAGE), 35% of patients on the approved dose had ARIA-E, and this was the most common finding at MRI. The most commonly reported symptom was headache. These trials also showed that the vast majority of these cases were clinically asymptomatic and that 98% of ARIA-E cases had resolved at

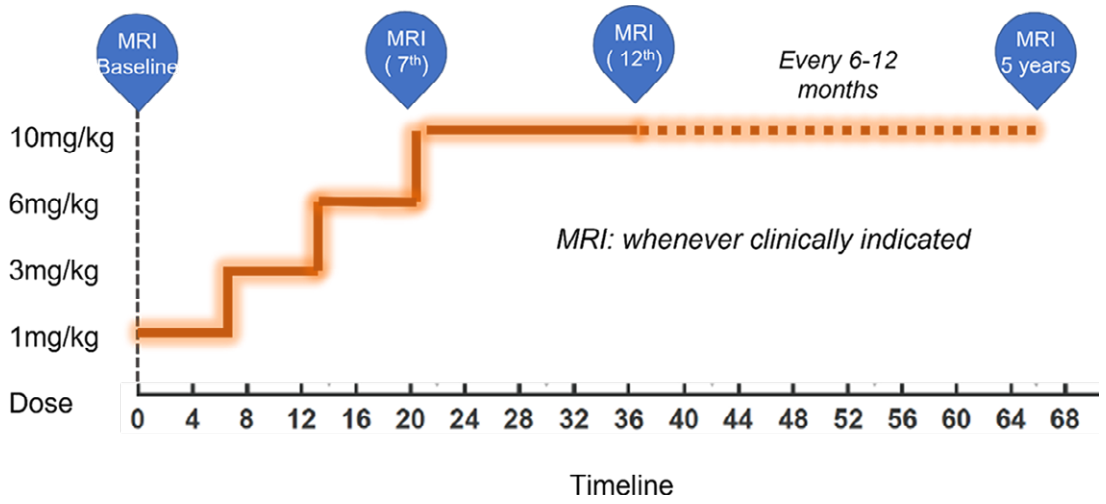

Figure 6. Dose titration chart and timeline (in weeks) for ARIA monitoring MRI. Current guidelines recommend starting at a low dose of 1 mg/kg for the first two infusions, moving to 3 mg/kg for the third and fourth infusions, 6 mg/kg for the fifth and sixth infusions, and finally to the optimum target dosage of 10 mg/kg from beyond the seventh infusion, usually achieved over a period of 20–24 weeks. MRI should be performed within 12 months before initiation of therapy and before the seventh (10 mg/kg dose) and 12th infusions for aducanumab, for up to 5 years. For *ApoE4* carriers, it is recommended to undergo MRI at the fifth (6 mg/kg), seventh (10 mg/kg), 10th, and 12th infusions. MRI should also be performed for any new signs or symptoms suggestive of ARIA or any other clinical indication.

Table 1: MRI Acquisition Protocol from ICARE-AD Study*

Imaging Sequence	Application
T2-weighted FLAIR (3D)	Imaging proteinaceous fluid in ARIA-E: Vasogenic edema in the parenchyma Effusion and exudate in the leptomeninges
T2*-weighted GRE	Imaging heme products in ARIA-H: microhemorrhage in the parenchyma, superficial siderosis in the leptomeninges
Diffusion-weighted imaging	Differential diagnosis
3D T1-weighted anatomic imaging (optional)	Facilitating postprocessing and assessment of disease progression

Source.—Reference 10.
* Schedule: baseline (pretreatment); posttreatment before the seventh and 12th infusions and every 6–12 months thereafter for up to 5 years. 3D = three-dimensional.

follow-up imaging. ARIA-E occurred most frequently between 3 and 6 months of treatment, with incidence sharply dropping after the first 9 months (4). Parenchymal edema is easily detected with T2-weighted FLAIR sequences and appears as cortical-subcortical areas of hyperintensity with mild gyral swelling and mass effect (Fig 7A, 7B). There is no parenchymal enhancement, although subtle leptomeningeal enhancement may sometimes be associated secondary to venous congestion. Unlike conditions with cytotoxic edema such as acute infarct, ARIA-E shows increased diffusion with high apparent diffusion coefficient values as expected along the lines of vasogenic edema (Fig 7B) (4,31,36,37).

Exudates within the sulci are also seen as FLAIR hyperintense signal and lack of CSF signal suppression, with or without enhancement (Fig 8). Edema and effusion may occur separately or together, with different studies showing different results for a higher incidence of either or both (5,9,32,36). These changes are most frequently seen in the occipital lobes, followed by the frontoparietal lobes, and are least common in the cerebellum (9,37). When edema and effusion coincide, they are usually seen in the same region rather than distant from each other (Fig 9). The grading of ARIA-E is dependent on the area of involvement and guides the decision on drug continuation. The grading is detailed in Table 2 (37,38). A single location with a less than 5-cm maximum dimension is graded as mild, whereas more than 10-cm (one or many) involvement is graded as severe (Fig 10). Most ARIA-E events (>80%) were asymptomatic and resolved with dose adjustment (4,31,36).

ARIA Hemorrhage

ARIA-H is characterized by parenchymal microhemorrhages and/or superficial siderosis, with the incidence around 15%–20% in most clinical trials (4,5,9,32,36). Microhemorrhages are more common than superficial siderosis and are defined as punctate rounded foci of signal dropout on the gradient sequences measuring less than 1 cm (Fig 11). Superficial siderosis manifests as curvilinear areas of signal dropout along

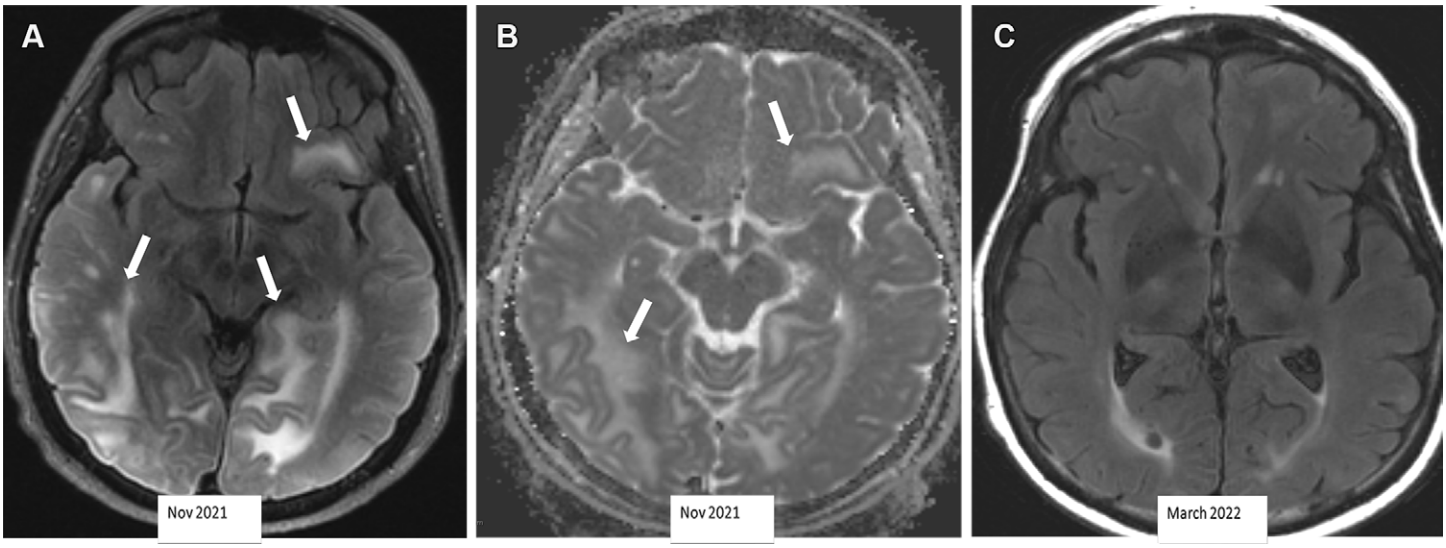

Figure 7. Severe ARIA-E (edema) in a 69-year-old woman receiving aducanumab therapy for AD with headaches and word-finding difficulty. **(A, B)** Axial MR images of the brain show multifocal subcortical edema (arrows) with FLAIR hyperintensity **(A)** and increased diffusion on the apparent diffusion coefficient (ADC) map **(B)**, with a few areas measuring more than 10 cm. **(C)** Axial follow-up MR image 4 months later shows near-complete resolution of signal intensity changes. ARIA-E is most common in the occipital lobes (as in this case) and mimics posterior reversible encephalopathy syndrome (PRES) at imaging.

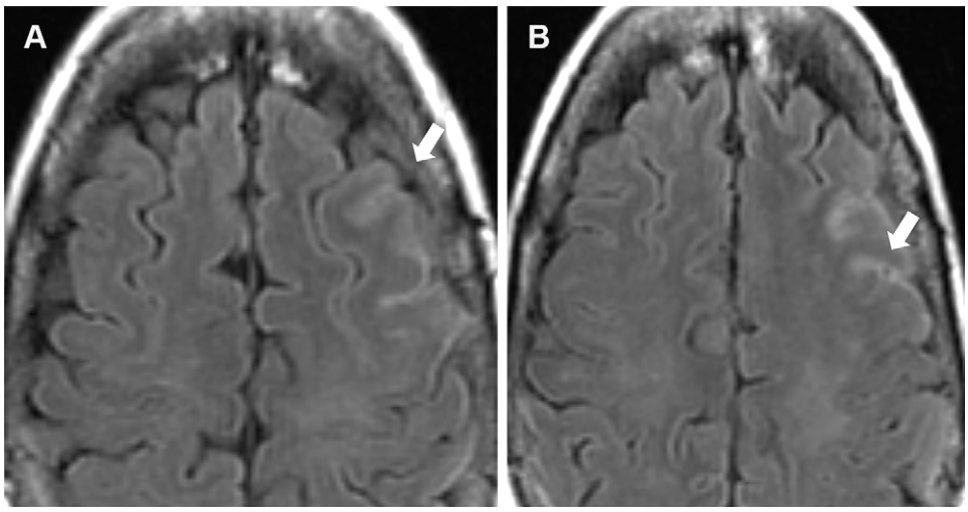

Figure 8. Mild ARIA-E (effusion) in a 62-year-old woman with mild cognitive impairment receiving aducanumab therapy. A baseline (pretreatment) MRI examination was unremarkable, and an amyloid PET examination (not shown) showed diffusely elevated amyloid. Contiguous axial FLAIR MR images obtained 9 weeks after initiation of therapy show sulcal hyperintensity (arrow) consistent with mild ARIA-E, and therapy was continued. Findings were stable at follow-up MRI after 1 month, with complete resolution after 3 months.

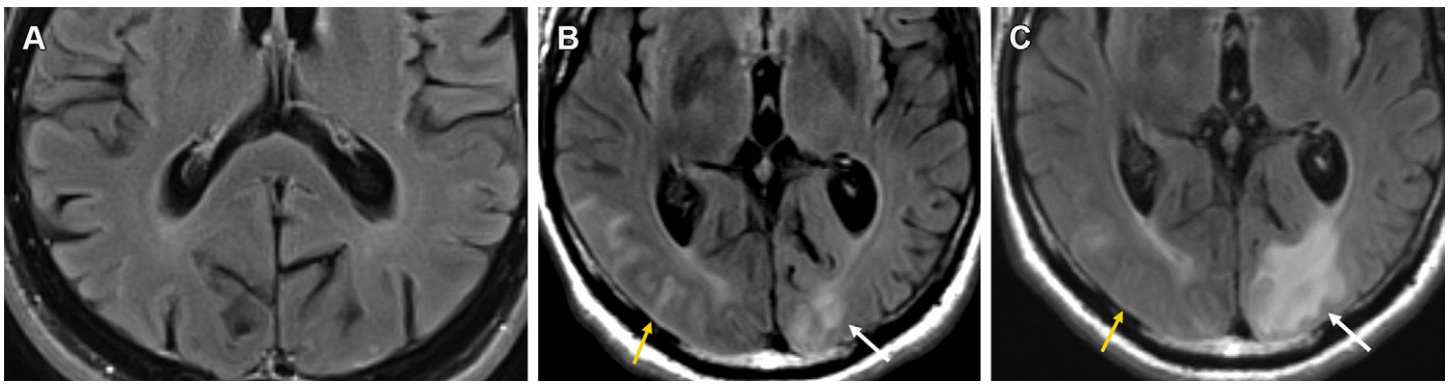

Figure 9. Mild ARIA-E (edema and effusion) in a 61-year-old man receiving aducanumab therapy. **(A, B)** Baseline pretreatment axial MR image **(A)** is unremarkable, with development of effusion **(B)** in the right occipital lobe (yellow arrow) and edema in the left occipital lobe (white arrow) on an axial MR image obtained 3 weeks after the target dose infusion (10 mg/kg). **(C)** Follow-up MR image after the fourth round of infusion shows near-complete resolution of the right occipital effusion (yellow arrow) with worsening of the left occipital lobe edema (white arrow). This was graded as mild throughout and therapy was continued, with complete resolution of all imaging changes at the seventh-week MRI examination.

Table 2: ARIA Grading Criteria

ARIA Type	Mild	Moderate	Severe
ARIA-E	FLAIR hyperintensity confined to sulcus and cortex/subcortical white matter in one location <5 cm	FLAIR hyperintensity 5–10 cm, or more than one site of involvement each measuring <10 cm	FLAIR hyperintensity >10 cm, often with sulcal involvement, may involve one or more sites
ARIA-H microhemorrhage	Four or more new microhemorrhages	Five to nine new microhemorrhages	10 or more new microhemorrhages
ARIA-H superficial siderosis	One focal area of superficial siderosis	Two focal areas of superficial siderosis	More than two focal areas of superficial siderosis

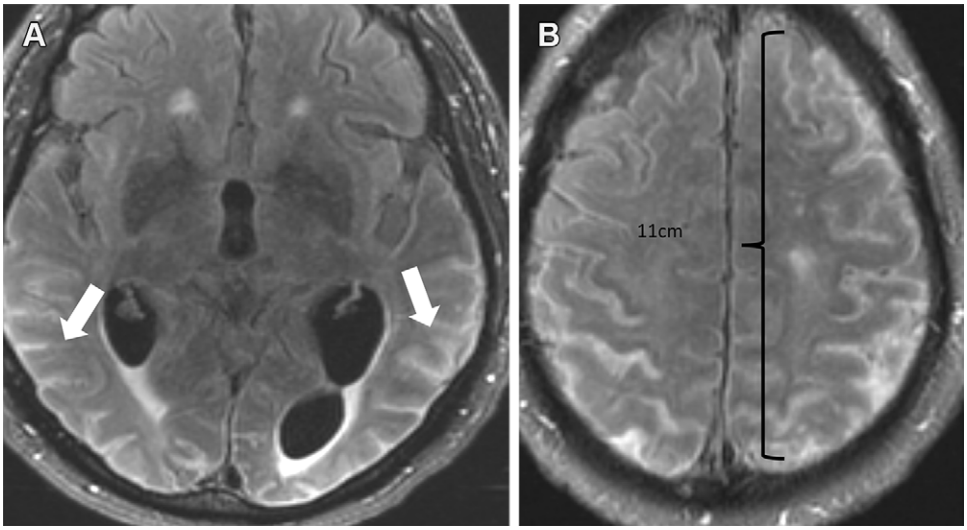

Figure 10. Severe ARIA-E (effusion) in a 76-year-old man with worsening headaches receiving aducanumab therapy for AD. Axial brain MR images from December 2021 (3 weeks after full dose) show multifocal exudates along the sulci with FLAIR hyperintensity (arrows in **A**), measuring more than 10 cm (severe) with subtle leptomeningeal enhancement **(B)**. Treatment was suspended, and complete resolution of effusion was noted after cessation of therapy.

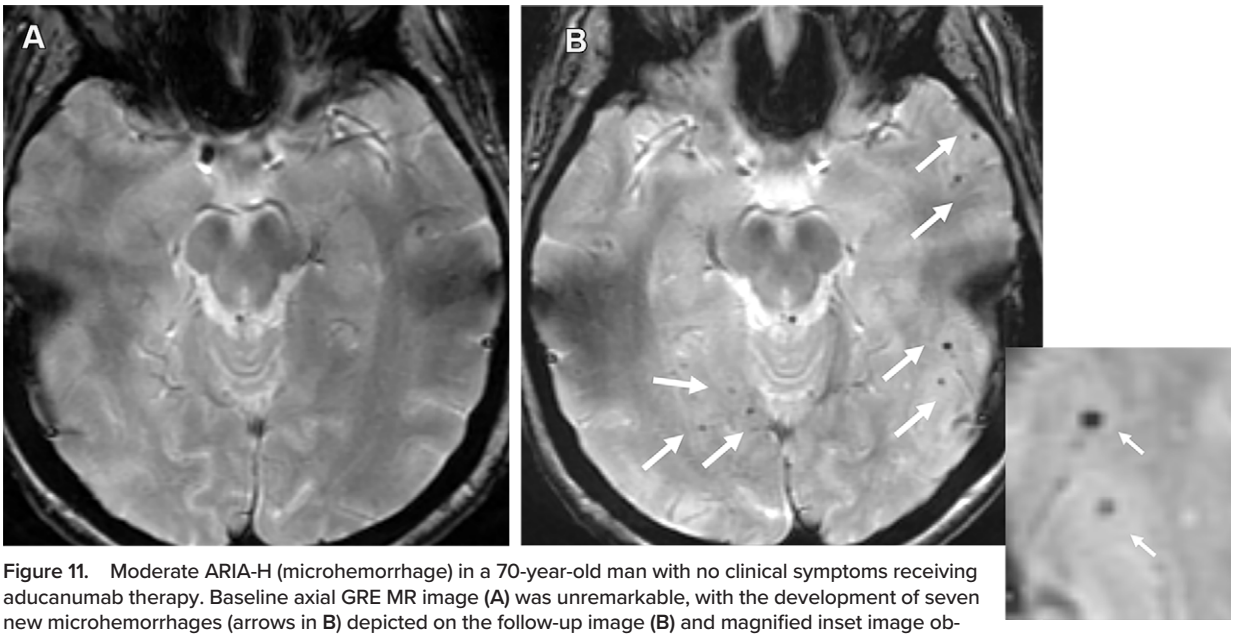

Figure 11. Moderate ARIA-H (microhemorrhage) in a 70-year-old man with no clinical symptoms receiving aducanumab therapy. Baseline axial GRE MR image **(A)** was unremarkable, with the development of seven new microhemorrhages (arrows in **B**) depicted on the follow-up image **(B)** and magnified inset image obtained 7 weeks after the target dose. Therapy was suspended for few weeks and was resumed following documentation of stable findings at follow-up MRI. It is important to maintain consistency in the sequence type (T2*-weighted GRE) and scanner type (all examinations performed with same strengths) as technical factors can result in miscounting of the number of microhemorrhages.

the brain surface and is the least common manifestation in the ARIA spectrum, frequently requiring cessation of therapy (Fig 12). The pathologic mechanism for both types of hemorrhage is identical, where disruption of the smooth muscle integrity of the vessel wall results in leakage of heme products into the parenchyma and sulci (8,9,35).

As the grading of severity is dependent on the number of microhemorrhages, careful assessment of the baseline number

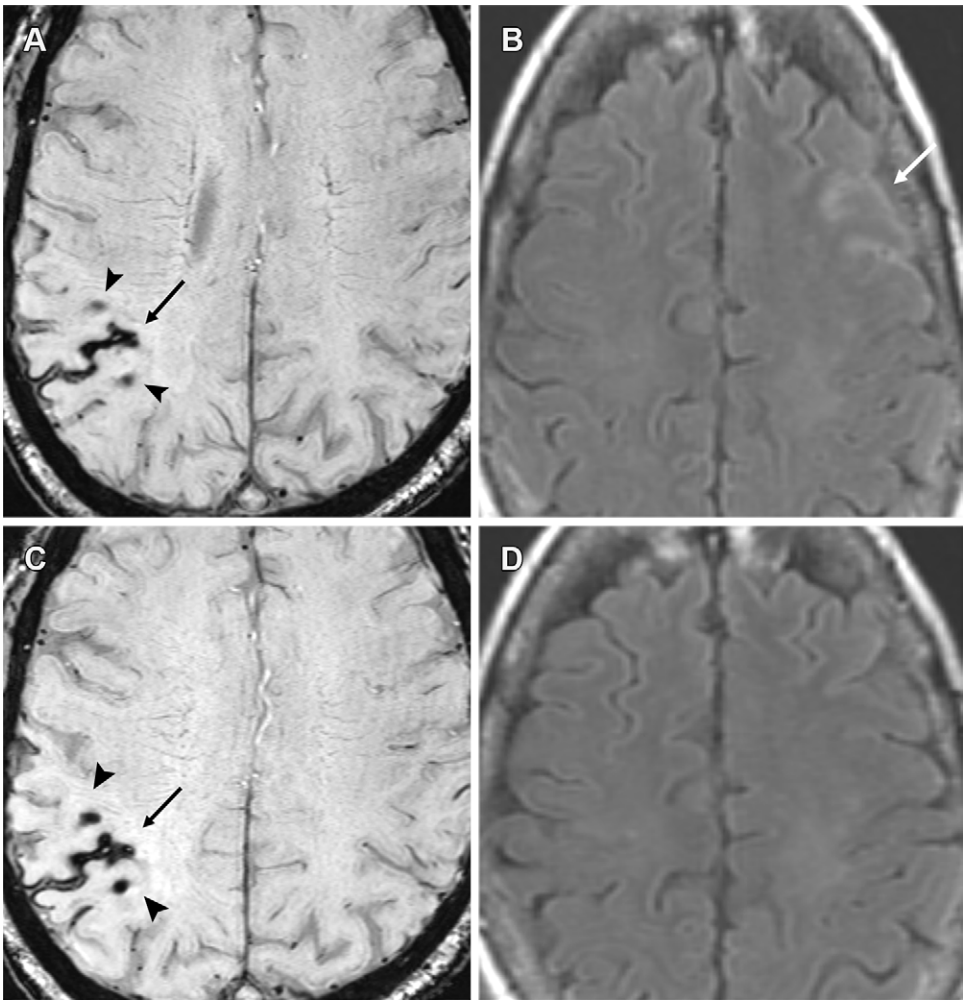

Figure 12. Moderate ARIA-E (edema) and ARIA-H (microhemorrhages, superficial siderosis) in a 60-year-old woman with headaches receiving aducanumab therapy. **(A, B)** Baseline MRI was unremarkable, with sequential MRI performed at 4 and 8 weeks after full dose. Axial T2*-weighted GRE **(A)** and FLAIR **(B)** MR images from the 4th-week examination show a new area of superficial siderosis (arrow in **A**), two microhemorrhages (arrowheads in **A**) in the right parietal convexity, and a subtle area of effusion (arrow in **B**) along the left frontal sulci. Therapy was suspended given the moderate radiographic findings and mild clinical symptoms. **(C, D)** Follow-up axial MR images at 8 weeks show stable hemorrhagic changes (arrow and arrowheads in **C**) on the T2*-weighted GRE image **(C)** with complete resolution of effusion on the FLAIR image **(D)**. Superficial siderosis is the least common manifestation of ARIA and can be symptomatic, frequently requiring temporary or complete cessation of therapy.

at pretreatment MRI is critical. Both types of hemorrhage are best seen with gradient and susceptibility-weighted sequences (39–41). Currently, the safety of aducanumab in patients with 10 or more brain microhemorrhages, pretreatment localized superficial siderosis, and/or with a brain hemorrhage greater than 1 cm within 1 year of treatment initiation has not been established; these patients are usually excluded from any clinical trials (4,8). The presence of four or fewer microhemorrhages or less than two focal areas of superficial siderosis will grade ARIA-H as mild, whereas 10 or more microhemorrhages or more than two areas of superficial siderosis will qualify it as severe (Table 2). Since counting the individual microhemorrhages is needed to grade the severity of ARIA-H, a standardized imaging protocol with consistency in the sequence and scanner is necessary. Susceptibility-weighted imaging, which offers higher spatial resolution, is now standard at most centers across all vendors (39–41). However, T2*-weighted GRE is still the recommendation per clinical trials.

Because increased vascular permeability forms the basis of both ARIA-E and ARIA-H, it is common for these entities to occur together as both fluid and heme products cross the damaged vessel wall. Some extent of fluid usually extravasates with blood, and it is postulated that some amount of ARIA-E almost always occurs with ARIA-H (Fig 13). However, the opposite is not true, and there is frequently no definite hemorrhagic leakage with fluid (4,8,9,36). Moreover, although edema resolves with time, the hemosiderin deposition is relatively fixed or may become less apparent with subsequent scans, which may be a confounding factor and lead to a spurious higher incidence of isolated ARIA-H (4). The interrelationship between ARIA-H and ARIA-E is also supported by the fact that, in many cases, new ARIA-H was seen in the location of prior ARIA-E before it occurred or after it had resolved. Nonetheless, these entities are graded separately, ultimately deciding the management, as discussed in the following section (37,38).

Differential Diagnosis and Interpretation Pitfalls

The term *inflammatory cerebral amyloid angiopathy* can be used as an umbrella term encompassing two subtypes: CAA-RI and amyloid β-related angiitis (AB-RA). As discussed earlier, there is a significant overlap between the pathophysiology of ARIA and CAA-RI (7,26,28). CAA-RI, considered a spontaneous human example of ARIA, is an autoimmune encephalopathy secondary to autoantibodies targeting Aβ protein deposited in the walls of cortical and leptomeningeal brain vessels.

Clinically, CAA-RI ranges from mild cognitive disturbances and headaches to rapidly progressive cognitive decline and seizures. This is a potentially reversible condition responsive to corticosteroid therapy (29). Imaging features

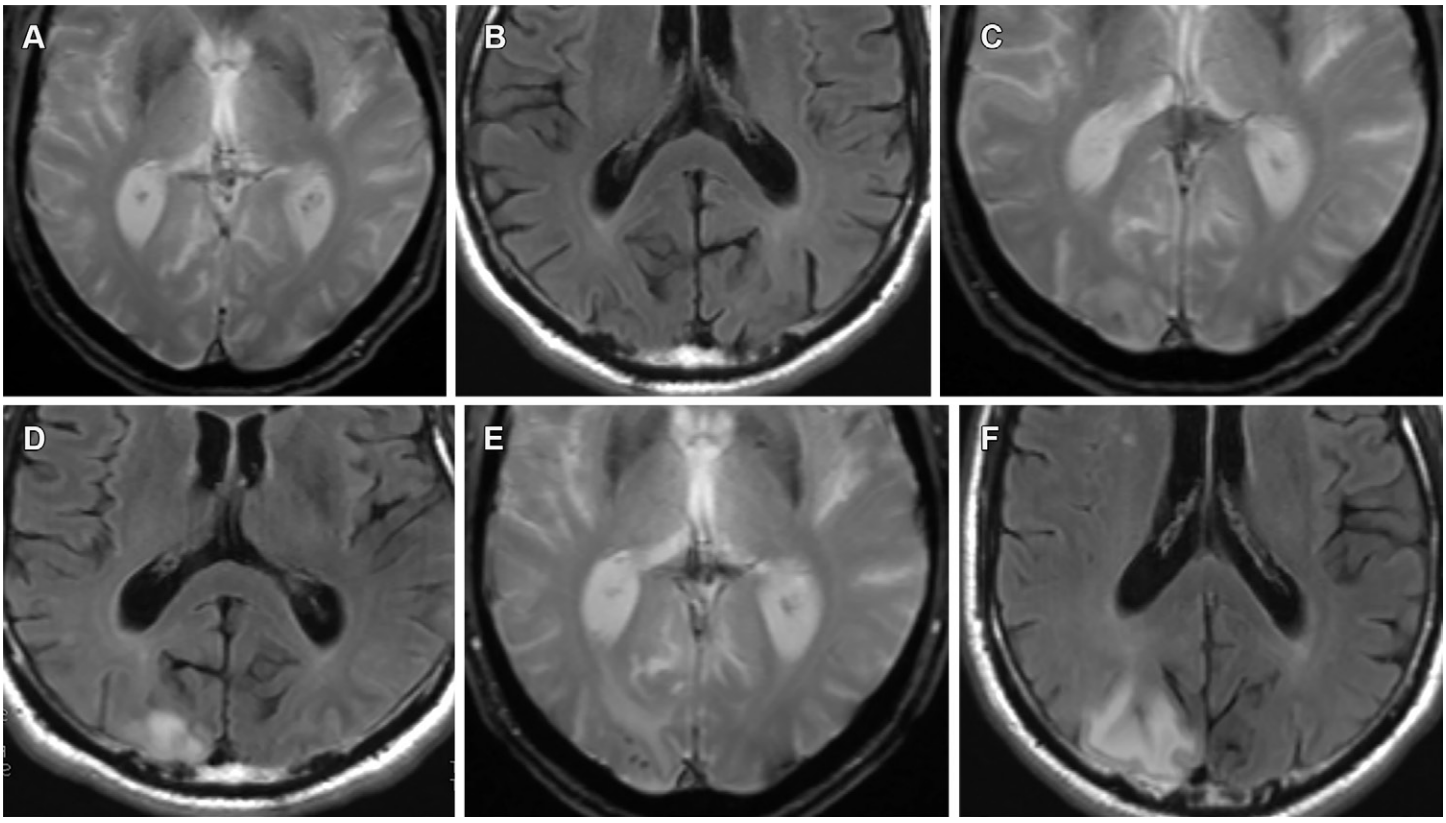

Figure 13. Mild ARIA-E (edema) and ARIA-H (microhemorrhage) in a 62-year-old woman with no clinical symptoms receiving aducanumab therapy. Sequential T2*-weighted GRE image and FLAIR MR images, respectively, are unremarkable at baseline **(A, B)**, show solitary microhemorrhage and mild edema at 4 weeks **(C, D)**, and show progression of edema and microhemorrhages after 8 weeks **(E, F)**. Although the edema is usually reversible, the microhemorrhages persist, as is seen on the follow-up MR images in this case. Edema and microhemorrhages can frequently coexist (ARIA-E+H) and are graded separately, with the therapy decision based on the highest grade of severity.

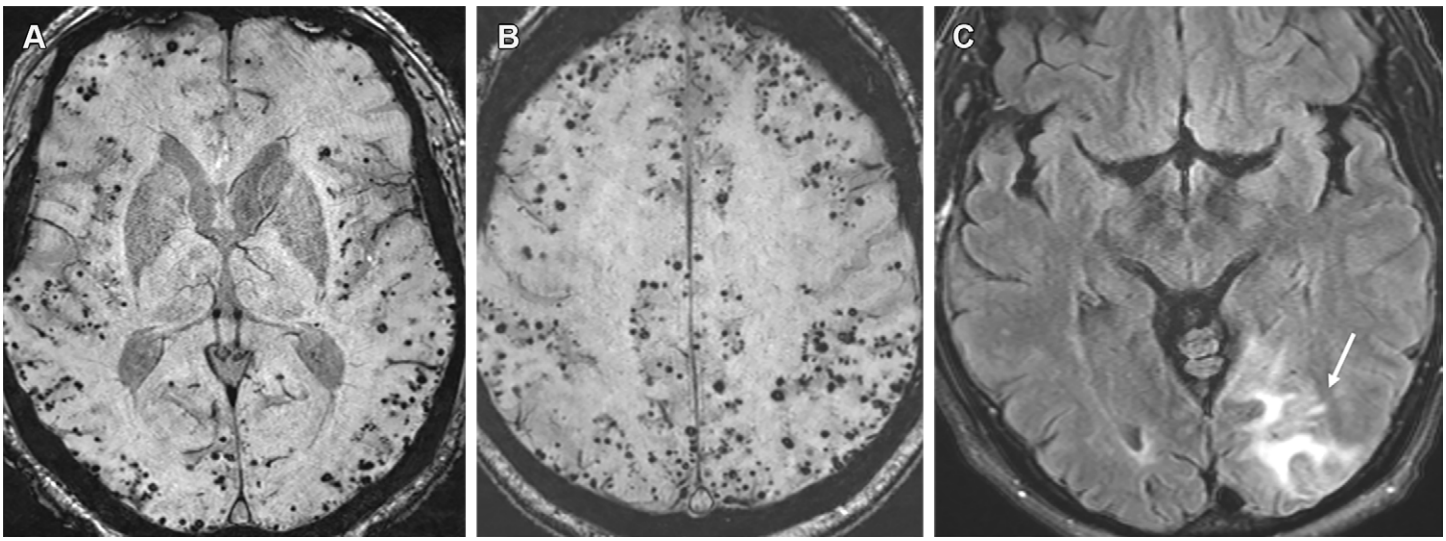

Figure 14. Advanced CAA with inflammatory changes (CAA-RI) in a 76-year-old man. **(A, B)** Axial susceptibility-weighted images show innumerable microhemorrhages in a peripheral lobar pattern. The patient subsequently presented to the emergency department with mental status changes, and MRI was performed. **(C)** Axial MR image shows cortical-subcortical edema (arrow) in the left occipital lobe consistent with acute inflammatory changes (CAA-RI). The imaging findings are indistinguishable from those of ARIA, and the differentiation is based primarily on clinical history. Moreover, patients with such a high number of microhemorrhages at pretreatment imaging are usually excluded from MAB clinical trials.

in CAA-RI include unifocal or multifocal areas of subcortical vasogenic edema with mild mass effect superimposed on a background of CAA (microhemorrhages, siderosis, and chronic parenchymal hematoma) (Fig 14). Imaging findings in CAA-RI are indistinguishable from those of ARIA, with the only difference being the clinical history of MAB administration (7,26,28,37). Because patients with significant background disease of CAA (five or more microhemorrhages) are

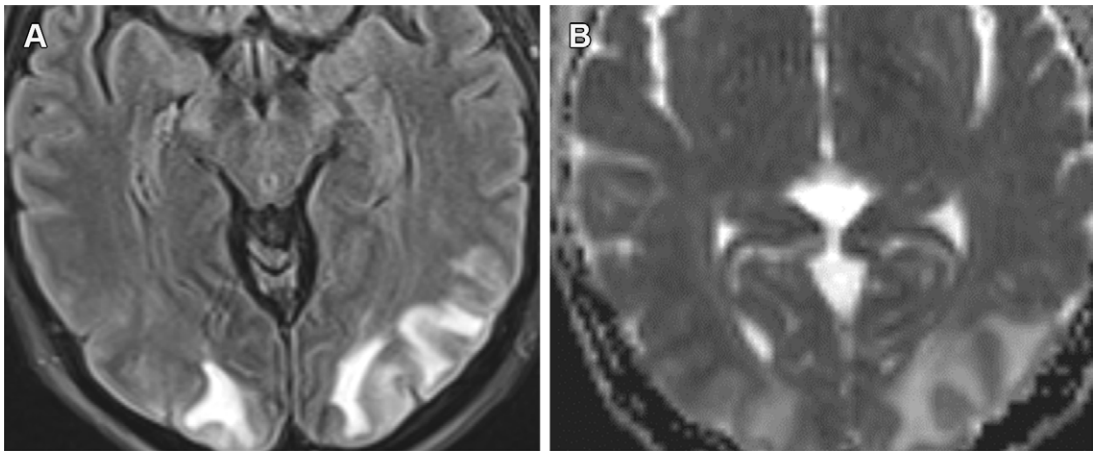

Figure 15. PRES secondary to hypertensive urgency with subcortical area of edema in the occipital lobes with FLAIR hyperintensity **(A)** and increased ADC values **(B)**. ARIA-E (edema) resembles PRES, with both having a predilection for the occipital lobes with the possibility of petechial hemorrhages. However, these conditions are distinguishable based on the clinical history, with PRES usually having an acute clinical presentation.

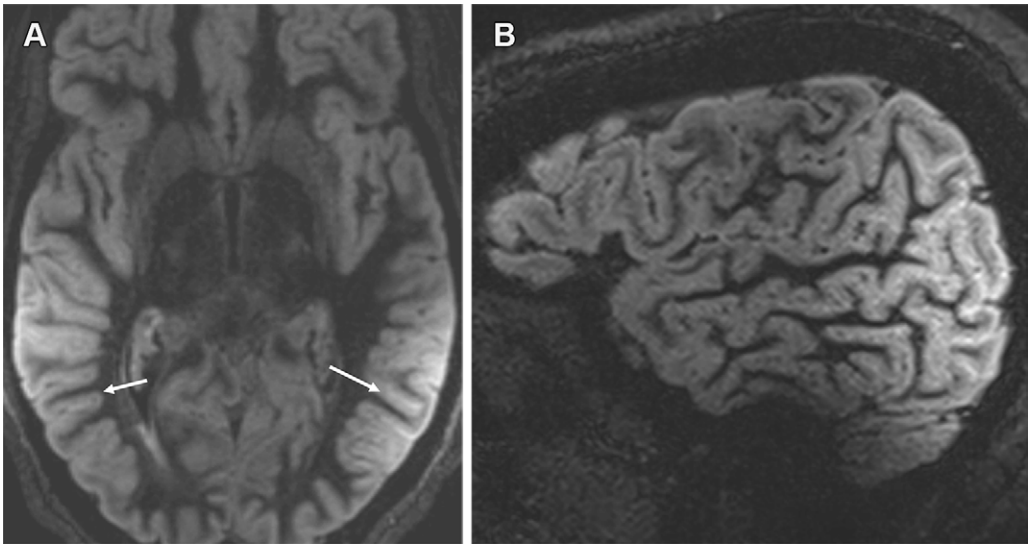

Figure 16. Shading artifact. Axial MR image **(A)** shows shading artifact with hyperintense signal within the sulci in the temporoparietal regions bilaterally (arrows in **A**) and loss of signal intensity in the frontal region on a sagittal direct inversion-recovery MR image **(B)**, secondary to improper coil placement. Numerous technical factors can cause artifactual FLAIR sulcal hyperintensity, which can mimic ARIA-E (effusion). However, it can sometimes be corrected by fixing the underlying cause, such as by adjusting to the proper size and loading of the coil or shimming to reduce inhomogeneity of the magnetic field.

excluded from MAB trials, any new area of vasogenic edema in patients receiving MAB is classified and treated as ARIA (4). As Aβ deposition forms the basis for both these conditions, future pretreatments or combination therapies with drugs tailored against CAA will likely lower the incidence of ARIA.

Apart from CAA-RI, other conditions in the imaging differential diagnosis for ARIA-E include posterior reversible encephalopathy syndrome (PRES), progressive multifocal encephalopathy, subacute infarcts, and vasculitis. Among these conditions, ARIA-E (edema) has a very striking resemblance to PRES, with both having a predilection for the occipital lobes with petechial hemorrhages and both being reversible (9,42–44) (Fig 15). These conditions are excluded based on clinical history, and to our knowledge there is no published literature in which these conditions were erroneously called ARIA. Confluent chronic small vessel ischemic (microangiopathic) changes can also mimic subtle areas of ARIA-E. However, these develop over a long period, and careful comparison with the pretreatment baseline MR images can help distinguish these two entities. Despite CAA being one of the most significant risk factors for ARIA, monitoring MRI for ARIA in patients with CAA should be interpreted the same way as for those in patients without CAA (28).

The imaging differential diagnosis for ARIA-E (effusion) includes a wide range of conditions that can cause sulcal FLAIR hyperintensity, including subarachnoid hemorrhage, meningitis, administration of supplemental oxygen, and technical factors like poor CSF signal suppression and susceptibility artifacts (37). Shading artifacts can occur when the patient is not centered in the receive coil, resulting in artifactually hyperintense areas (Fig 16). Differentiating most of these conditions from ARIA-E is usually straightforward as subarachnoid hemorrhage is picked up quickly at CT and meningitis is generally clinically evident. Artifactual causes secondary to underlying technical issues typically involve a broader region with a geographical band and associated parenchymal signal artifacts (8,9,37). These can be corrected by loading the coil correctly, by using the proper size coil for patient size, and shimming to reduce inhomogeneity of the

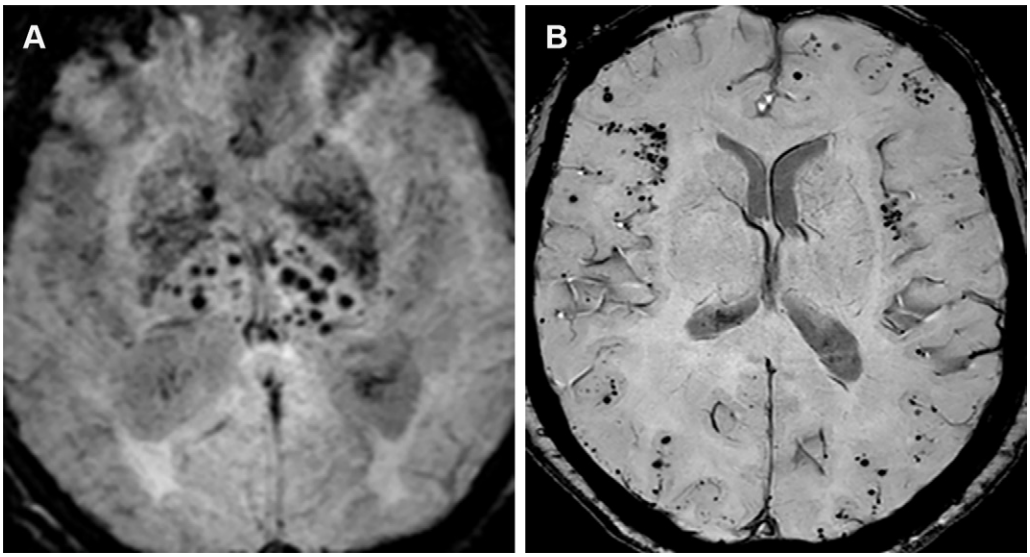

Figure 17. Hypertensive angiopathy and CAA are the two most common causes of cerebral microhemorrhages. Axial susceptibility-weighted image **(A)** shows a central pattern of microhemorrhages characteristic of hypertensive angiopathy, whereas on the axial susceptibility-weighted image **(B)**, amyloid angiopathy is characterized by a peripheral/lobar pattern.

magnetic field. Isolated ARIA-E (effusion) is uncommon as some parenchymal edema usually accompanies effusion in the same anatomic region (8).

The two most common causes of cerebral microhemorrhages are hypertensive and amyloid angiopathy. Both are associated with hemorrhagic and nonhemorrhagic imaging features such as cerebral microhemorrhages, cortical superficial siderosis, white matter hyperintensities, and expanded perivascular spaces (45,46). One of the most critical distinctions between these two entities is the predilection for location, which is peripheral and lobar in CAA and deep arteriolar in hypertensive angiopathy (Fig 17). CAA and hypertensive arteriopathy can occur together or separately in patients with AD, making monitoring for new microhemorrhages challenging (7,26,28,45). Many of these patients are already excluded from clinical trials due to the high number of microhemorrhages at the pretreatment screening examination (4,8). However, any new microbleed or siderosis in patients undergoing MAB therapy should be labeled ARIA-H. Counting the number of microhemorrhages can be a challenging but key component of ARIA assessment, further emphasizing the need for a standardized imaging protocol. Additionally, it is imperative to avoid counting physiologic iron deposition in the basal ganglia. Recent efforts have also been made to avoid counting microhemorrhages found in atypical locations of CAA, such as the brainstem and deep gray structures (more commonly associated with hypertension). Susceptibility-weighted imaging performed with the same magnet strength with thin sections should alleviate any issues of partial volumizing or confusing vessels for microhemorrhages (37,39,40).

ARIA-E should be the number one diagnostic consideration when parenchymal edema and/or sulcal FLAIR hyperintensity is seen in patients recently exposed to an amyloid-modifying MAB and in whom no evidence of any other inciting cause or underlying lesion can be found.

A multidisciplinary approach with a small core group of neurologists and neuroradiologists with knowledge about the technical aspects and imaging appearance forms the bottom line for successful aducanumab therapy implementation (3,4). It is imperative that radiologists are trained in the basics of the technical and scientific aspects of ARIA. Decisions on changes to aducanumab therapy should be based only on radiologic reports labeled as definite ARIA-H. Early ARIA-E findings can be subtle and easily missed on the initial images without any clinical consequences (4,8,9). In a retrospective review of multiple bapineuzumab trial studies, approximately 40% (15 of 36) of cases of asymptomatic ARIA-E were initially missed by the local readers, with patients remaining asymptomatic and continuing treatment after ARIA-E occurrence (36,47). It is critical not to misinterpret other pathologic conditions such as subarachnoid hemorrhage or PRES as advanced ARIA-E, which would necessitate cessation of therapy (28,37,42). Gradually, as more cases are seen and discussed over time, the radiologist will be more confident about their diagnosis.

Management of ARIA

When the findings of ARIA were noticed during the early part of clinical trials, it was stipulated that therapy must be permanently discontinued at imaging detection of ARIA. With broader usage and a better understanding of ARIA, most patients with asymptomatic ARIA meeting specific radiographic and clinical criteria may continue to receive treatment. Currently, the management of ARIA includes a combination of clinical symptomology and MRI grading severity (4,8,39). As ARIA-E is more common and usually transient, the vast majority of patients can continue therapy either with or without temporary suspension (Table 3). As depicted, therapy can be resumed even in the severe MRI stages of ARIA-E once the imaging findings resolve. Usually, temporary cessation of therapy works for almost all of the categories of ARIA-E, with few exceptions where steroid therapy might be needed (4,8). This is not true for the ARIA-H class, as even if it is asymptomatic, the detection of 10 or more new microhemorrhages (severe) requires permanent discontinuation of therapy (Table 4) (4,8). Findings of ARIA-H are irreversible, and no active treatment is currently approved for this.

Continuation of therapy in patients with ARIA relies heavily on the radiologist properly grading and monitoring the imaging

Table 3: Management of ARIA-E

	ARIA-E Severity at MRI		
Clinical Severity of ARIA-E	Mild	Moderate	Severe
Asymptomatic	Continue dosing at current dose and schedule	Suspend dosing; once imaging findings resolve, resume dose	Suspend dosing; once imaging findings resolve, resume dose
Mild, moderate, severe, serious ("other medically important event" only)	Suspend dosing; once ARIA-E resolves, same dose treatment can resume	Suspend dosing; once ARIA-E resolves, same dose treatment can resume	Suspend dosing; once ARIA-E resolves, same dose treatment can resume
Serious, except for "other medically important event"	Discontinue dosing	Discontinue dosing	Discontinue dosing

Source.—Reference 48.

Table 4: Management of ARIA-H

	ARIA-H Severity at MRI		
Clinical Severity of ARIA-H	Mild	Moderate	Severe
Asymptomatic	Continue dosing at current dose and schedule	Suspend dosing; once imaging findings resolve, resume dose	Discontinue
Mild, moderate, severe, serious ("other medically important event" only)	Suspend dosing; once ARIA-H resolves, same dose treatment can resume	Suspend dosing; once ARIA-H resolves, same dose treatment can resume	Suspend dosing; once ARIA-H resolves, same dose treatment can resume
Serious, except for "other medically important event"	Discontinue dosing	Discontinue dosing	Discontinue dosing

Source.—Reference 48.

findings. In many cases, therapy may continue in asymptomatic patients. ARIA-E is more transient, and therapy may continue or be temporarily stopped; stoppage of therapy in patients with ARIA-H depends on the severity and whether it is stabilized.

Conclusion

As with multiple other neurologic conditions, immunotherapy is becoming more prevalent in managing dementia, with recently approved MAB therapy being an exciting new frontier. The most common side effects of MABs include ARIA-E and ARIA-H, which share a common mechanism of vessel leakage. Ascertainment of ARIA plays a vital role in safety monitoring and management decisions in antiamyloid MAB trials and clinical practice. A conservative monitoring plan should be established with a multidisciplinary approach, which includes neurologists and radiologists familiar with the clinical and imaging aspects of ARIA.

Author affiliations.—From the Departments of Radiology (A.A., V.G., P.B., A.D.) and Neuroradiology (P.V.), Mayo Clinic, 4500 San Pablo Rd, Jacksonville, FL 32224; Mallinckrodt Institute of Radiology, Washington University School of Medicine, St. Louis, Mo (N.J.M.); and Department of Radiology, Mayo Clinic, Rochester, Minn (G.B.). Presented as an education exhibit at the 2022 RSNA Annual Meeting. Received January 16, 2023; revision requested May 8 and received June 11; accepted June 21. **Address correspondence to** A.A. (email: *amitmamc@gmail.com*).

Disclosures of conflicts of interest.—**A.A.** Consultant and expert witness for Authentic 4D, Michigan 2020; support for attending meetings and/or travel from institutional CME fund; stocks in Gilead Inc. **N.J.M.** Institutional grant from the Alzheimer's Association (AARF-D-20-681815). **G.B.** Grants through Foundation of Sarcoidosis Research, American Cancer Society, and Siemens Healthcare, unrelated to current work.

References

1. Lane CA, Hardy J, Schott JM. Alzheimer's disease. Eur J Neurol 2018;25(1):59–70.
2. Breijyeh Z, Karaman R. Comprehensive Review on Alzheimer's Disease: Causes and Treatment. Molecules 2020;25(24):5789.
3. Cummings J, Aisen P, Apostolova LG, Atri A, Salloway S, Weiner M. Aducanumab: Appropriate Use Recommendations. J Prev Alzheimers Dis 2021;8(4):398–410.
4. Salloway S, Chalkias S, Barkhof F, et al. Amyloid-Related Imaging Abnormalities in 2 Phase 3 Studies Evaluating Aducanumab in Patients With Early Alzheimer Disease. JAMA Neurol 2022;79(1):13–21.
5. Swanson CJ, Zhang Y, Dhadda S, et al. A randomized, double-blind, phase 2b proof-of-concept clinical trial in early Alzheimer's disease with lecanemab, an anti-Aβ protofibril antibody. Alzheimers Res Ther 2021;13(1):80 [Published correction appears in Alzheimers Res Ther 2022;14(1):70.]
6. van Dyck CH, Swanson CJ, Aisen P, et al. Lecanemab in Early Alzheimer's Disease. N Engl J Med 2023;388(1):9–21
7. Antolini L, DiFrancesco JC, Zedde M, et al. Spontaneous ARIA-like Events in Cerebral Amyloid Angiopathy-Related Inflammation: A Multicenter Prospective Longitudinal Cohort Study. Neurology 2021;97(18):e1809–e1822.
8. Cogswell PM, Barakos JA, Barkhof F, et al. Amyloid-Related Imaging Abnormalities with Emerging Alzheimer Disease Therapeutics: Detection and Reporting Recommendations for Clinical Practice. AJNR Am J Neuroradiol 2022;43(9):E19–E35.
9. Sperling RA, Jack CR Jr, Black SE, et al. Amyloid-related imaging abnormalities in amyloid-modifying therapeutic trials: recommendations from the Alzheimer's Association Research Roundtable Workgroup. Alzheimers Dement 2011;7(4):367–385.
10. Defining a Standardized MRI Acquisition Protocol to Be Proposed to ICARE AD Sites for ARIA Monitoring (N3. 001). Presented at N1 - Neuroscience in the Clinic: Aducanumab: From Clinical Trials to the Clinic. American Academy of Neuroradiology 2022.

11. Forloni G, Artuso V, La Vitola P, Balducci C. Oligomeropathies and pathogenesis of Alzheimer and Parkinson's diseases. Mov Disord 2016;31(6):771–781.
12. Hardy J, Selkoe DJ. The amyloid hypothesis of Alzheimer's disease: progress and problems on the road to therapeutics. Science 2002;297(5580):353–356.
13. Jin M, Shepardson N, Yang T, Chen G, Walsh D, Selkoe DJ. Soluble amyloid beta-protein dimers isolated from Alzheimer cortex directly induce Tau hyperphosphorylation and neuritic degeneration. Proc Natl Acad Sci U S A 2011;108(14):5819–5824.
14. Selkoe DJ, Hardy J. The amyloid hypothesis of Alzheimer's disease at 25 years. EMBO Mol Med 2016;8(6):595–608.
15. Jack CR Jr, Bennett DA, Blennow K, et al; Contributors. NIA-AA Research Framework: Toward a biological definition of Alzheimer's disease. Alzheimers Dement 2018;14(4):535–562.
16. Jack CR Jr, Knopman DS, Jagust WJ, et al. Hypothetical model of dynamic biomarkers of the Alzheimer's pathological cascade. Lancet Neurol 2010;9(1):119–128.
17. Dubois B, Hampel H, Feldman HH, et al; Proceedings of the Meeting of the International Working Group (IWG) and the American Alzheimer's Association on "The Preclinical State of AD"; July 23, 2015; Washington DC, USA. Preclinical Alzheimer's disease: Definition, natural history, and diagnostic criteria. Alzheimers Dement 2016;12(3):292–323.
18. Clark CM, Schneider JA, Bedell BJ, et al; AV45-A07 Study Group. Use of florbetapir-PET for imaging β-amyloid pathology. JAMA 2011;305(3):275–283.
19. Fleisher AS, Chen K, Liu X, et al. Using positron emission tomography and florbetapir F18 to image cortical amyloid in patients with mild cognitive impairment or dementia due to Alzheimer disease. Arch Neurol 2011;68(11):1404–1411.
20. Ikonomovic MD, Klunk WE, Abrahamson EE, et al. Post-mortem correlates of in vivo PiB-PET amyloid imaging in a typical case of Alzheimer's disease. Brain 2008;131(Pt 6):1630–1645.
21. Roberts BR, Lind M, Wagen AZ, et al. Biochemically-defined pools of amyloid-β in sporadic Alzheimer's disease: correlation with amyloid PET. Brain 2017;140(5):1486–1498.
22. Altomare D, Caprioglio C, Assal F, et al. Diagnostic value of amyloid-PET and tau-PET: a head-to-head comparison. Eur J Nucl Med Mol Imaging 2021;48(7):2200–2211.
23. Ossenkoppele R, Rabinovici GD, Smith R, et al. Discriminative Accuracy of [18F]flortaucipir Positron Emission Tomography for Alzheimer Disease vs Other Neurodegenerative Disorders. JAMA 2018;320(11):1151–1162.
24. Higuchi M. Tau PET Imaging. Adv Exp Med Biol 2019;1184:217–230.
25. Nicoll JA, Wilkinson D, Holmes C, Steart P, Markham H, Weller RO. Neuropathology of human Alzheimer disease after immunization with amyloid-beta peptide: a case report. Nat Med 2003;9(4):448–452.
26. Kim SH, Ahn JH, Yang H, Lee P, Koh GY, Jeong Y. Cerebral amyloid angiopathy aggravates perivascular clearance impairment in an Alzheimer's disease mouse model. Acta Neuropathol Commun 2020;8(1):181.
27. Boche D, Zotova E, Weller RO, et al. Consequence of Abeta immunization on the vasculature of human Alzheimer's disease brain. Brain 2008;131(Pt 12):3299–3310.
28. Greenberg SM, Bacskai BJ, Hernandez-Guillamon M, Pruzin J, Sperling R, van Veluw SJ. Cerebral amyloid angiopathy and Alzheimer disease - one peptide, two pathways. Nat Rev Neurol 2020;16(1):30–42.
29. Eng JA, Frosch MP, Choi K, Rebeck GW, Greenberg SM. Clinical manifestations of cerebral amyloid angiopathy-related inflammation. Ann Neurol 2004;55(2):250–256.
30. Scolding NJ, Joseph F, Kirby PA, et al. Abeta-related angiitis: primary angiitis of the central nervous system associated with cerebral amyloid angiopathy. Brain 2005;128(Pt 3):500–515.
31. Sperling RA. Risk Factors and Clinical Course Associated with Vasogenic Edema fin a Phase II Trial of Bapineuzumab. In: Neurology. Philadelphia, PA: Lippincott Williams & Wilkins, 2009.
32. Bohrmann B, Baumann K, Benz J, et al. Gantenerumab: a novel human anti-Aβ antibody demonstrates sustained cerebral amyloid-β binding and elicits cell-mediated removal of human amyloid-β. J Alzheimers Dis 2012;28(1):49–69.
33. Sevigny J, Chiao P, Bussière T, et al. The antibody aducanumab reduces Aβ plaques in Alzheimer's disease. Nature 2016;537(7618):50–56.
34. Barakos J, Purcell D, Suhy J, et al. Detection and Management of Amyloid-Related Imaging Abnormalities in Patients with Alzheimer's Disease Treated with Anti-Amyloid Beta Therapy. J Prev Alzheimers Dis 2022;9(2):211–220.
35. Brashear HR, Ketter N, Bogert J, Di J, Salloway SP, Sperling R. Clinical Evaluation of Amyloid-Related Imaging Abnormalities in Bapineuzumab Phase III Studies. J Alzheimers Dis 2018;66(4):1409–1424.
36. Black RS, Sperling RA, Safirstein B, et al. A single ascending dose study of bapineuzumab in patients with Alzheimer disease. Alzheimer Dis Assoc Disord 2010;24(2):198–203.
37. Barakos J, Sperling R, Salloway S, et al. MR imaging features of amyloid-related imaging abnormalities. AJNR Am J Neuroradiol 2013;34(10):1958–1965.
38. Barkhof F, Daams M, Scheltens P, et al. An MRI rating scale for amyloid-related imaging abnormalities with edema or effusion. AJNR Am J Neuroradiol 2013;34(8):1550–1555.
39. Haacke EM, Xu Y, Cheng YC, Reichenbach JR. Susceptibility weighted imaging (SWI). Magn Reson Med 2004;52(3):612–618.
40. Haller S, Haacke EM, Thurnher MM, Barkhof F. Susceptibility-weighted Imaging: Technical Essentials and Clinical Neurologic Applications. Radiology 2021;299(1):3–26.
41. Kirsch W, McAuley G, Holshouser B, et al. Serial susceptibility weighted MRI measures brain iron and microbleeds in dementia. J Alzheimers Dis 2009;17(3):599–609.
42. Stott VL, Hurrell MA, Anderson TJ. Reversible posterior leukoencephalopathy syndrome: a misnomer reviewed. Intern Med J 2005;35(2):83–90.
43. Tungkasaereerak C, Phanthumchinda K. Reversible posterior leukoencephalopathy syndrome: a retrospective study in King Chulalongkorn Memorial Hospital. J Med Assoc Thai 2008;91(3):427–432.
44. Schiff D, Lopes MB. Neuropathological correlates of reversible posterior leukoencephalopathy. Neurocrit Care 2005;2(3):303–305.
45. Viswanathan A, Chabriat H. Cerebral microhemorrhage. Stroke 2006;37(2):550–555.
46. Haller S, Vernooij MW, Kuijer JPA, Larsson EM, Jäger HR, Barkhof F. Cerebral Microbleeds: Imaging and Clinical Significance. Radiology 2018;287(1):11–28.
47. Stehling C, Wersching H, Kloska SP, et al. Detection of asymptomatic cerebral microbleeds: a comparative study at 1.5 and 3.0 T. Acad Radiol 2008;15(7):895–900.
48. LEQEMBI (lecanemab). Prescribing information. LEQEMBI. https://www.leqembi.com/-/media/Files/Leqembi/Prescribing-Information.pdf. Accessed July 26, 2023.